Check for updates

# Method to map human and infrastructure vulnerability using CNN land cover: Case study of floating tank explosion at petrochemical plants of LaemChabang, Thailand

T. Sentagne [a], M. Zerbola [a], M. Garcia [a], C. Kumsap [b], V. Mungkung [b], L. Mezeix [c,*]

[a] *Université de Toulouse, INSA, UPS, Mines d'Albi, ISAE, ICA (Institut Clément Ader), 135 Avenue de Rangueil, Cedex, 31077, Toulouse, France*
[b] *Defence Technology Institute, 47/433 Moo 3, Ban Mai, Pak Kret, Nonthaburi, 11120, Thailand*
[c] *Faculty of Engineering, Burapha University, 169 Long-Hard Bangsaen Road, Chonburi, 20131, Thailand*

## ABSTRACT

Industrial storage tanks, used to store flammable materials in the petrochemical industry, can induce potential fire and explosion under specific conditions. Therefore, it is necessary to map the population and environment vulnerability, and, to develop procedures for emergency responses in order to reduce potential casualties. In order to achieve this, Convolutional Neural Networks (CNN) are used in this study using 6 classes: floating tank, forest, house, road, wasteland and water. Datasets are built for a total of approximately 1.4 million tiles with a resolution of 0.33m/pixel and their size are optimized in function of the class. The 6 associated CNN models are built and optimized to classify each class. The validation of the models shows that, with the exception of road and wasteland where the precision is only 73% and 89% respectively, the other 4 classes have a value higher than 95%. Post-processing is performed on each prediction before aggregating these results to obtain the land cover. For the floating tank class, a 5 step post-processing is used based on a Density-Based Spatial Clustering of Applications with Noise algorithm (DBCAN) after which blast simulation is applied and effects on people, buildings and trees are obtained through 4 steps. Finally, the petrochemical site of LaemChabang in Thailand is used as study case. Except for the road class that is difficult to detect, land cover is well performed. Human casualties and surface of damaged buildings are finally estimated demonstrating the usefulness of the tool to be used for the emergency planning of industrial disasters.

## 1. Introduction

Industrial storage tanks are equipment used to store gas, oil and petrochemical products, employed for oil and petrochemical industries. They have the potential to cause major hazards, because of their dangerous features, huge volume and close layout. Flammable materials can induce, under specific conditions, fire and explosion accidents creating blast waves and thermal radiation and causing casualties, infrastructure damages, pollution to the environment and economic losses. Even if safety is the highest concern of the petrochemical industry, nevertheless, accidents may occur and their prevention aims at limiting their consequences. Improper emergency response can cause casualties (death and injuries) and huge amount of economic losses. In 2016, more than seven foreign accidents caused 47 deaths and 151 injuries (Recycling Business Network, 2017). 41 deaths, 16 injuries, and

direct economic losses of 172.37 million yuan have been the results of the Chinese petrochemical industry accident in 2017 (Enterprise Security Assistant, 2019). Therefore, emergency response as SEVESO Directives in Europe (European Council, 1982) must be prepared in order to plan the emergency response.

Evaluation and mapping of the population and environmental vulnerability around hazardous industrial sites is necessary for an effective preparedness and to reduce casualties and infrastructure damage. Areal Locations of Hazardous Atmosphere (ALOHA) and Geographical Information System (GIS) approaches are used to evaluate the vulnerability of population near the industrial area (Ma et al., 2013; Cheng et al., 2015; Anjana et al., 2015; Rahman et al., 2015; Anjana et al., 2018; Khanmohamadi et al., 2018; Nilambar et al., 2016; Lucyna, 2016). Evaluation and mapping of human and environmental vulnerability to accidental release of hazardous chemicals has been analyzed

---

(Rajeev et al., 2019). Blast waves and thermal radiation due to the explosion have been simulated and casualties and damage have been mapped. Moreover, an evacuation route map was proposed thanks to a network analysis technique of GIS which is a powerful tool to determine the risk and population vulnerability assessment. However, a large number of GIS database layers have to be prepared, usually from LULC (Land use –Land cover). In order to establish the right emergency response, automatic detection of storage tanks and the surrounding environment are critical information.

Different unsupervised methods have been initially proposed to detect circular-shaped oil tanks. Morphological and segmentation methods to detect bright tanks were used (Kushwaha et al., 2013). Hough transform was applied to detect tanks (Cai et al., 2014), while a combination of quasi-circular shadows and highlighting arcs to detect oil tanks in synthetic aperture radar images (Xu et al., 2014). A salient region method for image segmentation and geometric features were employed for reducing the false alarms (Yao et al., 2014). Chord-to-point distance accumulation proposed by (Awrangjeb and Lu, 2008) has been used by (Ok, 2014) and the symmetric nature of the circular oil depots has been considered by (Ok and Emre, 2015). However, these different methods have shown limitations as they detect tanks based on the shapes and colors and so multi-type tank detection is not possible. To perform it deep learning methods have been used with remote sensing images. Object detection took advantage of Convolutional Neural Network (CNN) and are used in many fields as medicine (Loh et al., 2021), industry process (Xiao et al., 2021), mining (Kanghui et al., 2021) or storage tanks (Li and Wu, 2019; Li et al., 2022). Storage tank detection process can be generally divided into 3 steps: object detection, feature extraction and classification (Huang and Zhang, 2013; Li and Itti, 2011; Zhang et al., 2015). Zhang et al. (2015) proposed a CNN used to extract surrounding features of oil tanks combined with histogram of Oriented Gradients method to extract the shape information for local areas. Five major problems were reported as follows: (1) effect of image contrast; (2) image resolution; (3) effect of tank dimensions and shape; (4); complex images with various objects and (5) conversion of the true-color image to the greyscale. In order to improve the performance a 4-stage process was proposed: region of interest extraction, circular object detection, feature extraction, and classification (Jivane and Rajkumar, 2017, Moein et al., 2019). The Otsu's threshold method has been used to determine the region of interest (Jivane and Soundrapandiyan, 2017). Then, a speeded up robust features (SURF) technique was applied for the detection. Next, features extractions as Histogram Oriented Gradient was used for the extraction. Finally, classification was performed using a Support Vector Machine. Moein et al. (2019) used an improved Faster Region Based Convolutional Neural Networks (R–CNN) to extract the regions of interest and a fast circle detection technique for the detection. Higher detection rate than other feature-based methods was obtained with the 4-step method. However, these researches are limited to the storage tank detection. Surrounding environment has not been investigated that is necessary to collect data in order to be able to perform the vulnerability map.

By using CNN land cover, vulnerability mapping can be greatly facilitated. Indeed, by analyzing the prediction, information can be extracted and used in different external models to simulate damage, casualties, effect of blasts. Moreover, using this approach the number of database sources required can be reduced. It has been demonstrated that CNN for land cover has a higher predictive capability than the other classification algorithms such as: Support Vector Machine (SVM), Random Forest (RF), logistic regression and other similar methods (Cheolhee et al., 2019; Fernanda et al., 2020; Ma et al., 2019; Li et al., 2019; Mahdi et al., 2020). Different classification can be performed using CNN, such as agricultural land (Bhosle and Musande, 2019), tree mortality (Jean-Daniel et al., 2019), urban coastal zones (Lu et al., 2018), urban growing (Ruiz Emparanza et al., 2020; Chermprayong et al., 2020) or rural and urban area (Fitton et al., 2021; Mentet et al., 2022). However, land cover enables to characterize only the external

physical attributes of the land/object (size and distance). To estimate an effect or a consequence of a tank explosion, it is necessary to combine the land cover with the explosion model. However, despite the obvious interest of the topic, the authors have found no papers on this subject.

The aim of this work is to propose an automatic tool to support the emergency in their response planning in order to reduce the potential casualties. The objectives are to create a land cover of petrochemical plants and surrounding environment using CNN models and to map the population and infrastructure vulnerability from a storage tank explosion. The challenge of this work is to obtain an accurate land cover and to extract data from it that can be applied as inputs of the explosion model. In order to achieve it, a dataset based on 6 classes: floating storage tank, forest, house, road, wasteland and water, is built. Then, methodology to create the land cover and to simulate a storage tank explosion is described. An application of the methodology to a practical use case is performed and detailed step by step. Human casualties and injuries as well as the number of damaged buildings are estimated. Moreover, potential roads blocked by fallen trees are simulated. Finally, model limitations and perspective are discussed. As observed, the advantage of the proposed solution is from a single data source, i.e. a remote sensing image, to be able to provide all information needed for authorities.

## 2. Case study

### 2.1. Industrial fuel storage tank in Thailand

Industrial fuel storage tanks or petroleum tanks, can store various fluids. They are used in the petroleum and chemical industries to store both raw materials and intermediate or finished products. They are classified as three main types (Chem, 2008): Fixed roof tanks, floating roof tanks and fixed roof tanks with internal floating roof. As the floating roof tank is one of the most commonly used in Thailand, work focuses on this type (Fig. 1a). Tanks are normally separated from the rest of the installation for safety reasons. However, due to the rapid urban expansion, buildings can be built at a distance lower than 300 m (Fig. 1b), that is the distance from the leakage point where vapor cloud ignites (Knegtering and Pasman, 2009).

### 2.2. Dataset

To perform the land cover of petrochemical plants and surroundings environment 6 classes have been investigated: floating storage tank, forest, house, road, wasteland and water (Table 1). Satellite images are collected from the Sentinel images in 2022. To obtain the adequate level of precision, a definition of 0.33 m per pixel is chosen. A large number of satellite images are used to create the dataset tiles. The choice of the tile size is a critical point in order to maintain a significantly bigger context (Mnih and Hinton, 2010; Basu et al., 2015). Therefore, tiles size has been optimized for each class (Table 1), and examples are given in Fig. 2. Several researches demonstrated that a large dataset is required to reach an accuracy higher than 90%, (Ruiz Emparanza et al., 2020; Chermprayong et al., 2020; Fitton et al., 2021; Mentet et al., 2022). In the current work an average of 230,000 tiles per class is produced (Table 1). Each class is associated to a specific CNN model and, therefore, 6 datasets must be organized. Each dataset is built around two sub-classes: the investigated one and the other one that consists of everything except the investigated one (Table 1). As recommended in the literature, 70% of the total tiles have been randomly selected as a training set, and 15% for both validation and testing sets (Cihan et al., 2021; Xie et al., 2021; Elmaz et al., 2021).
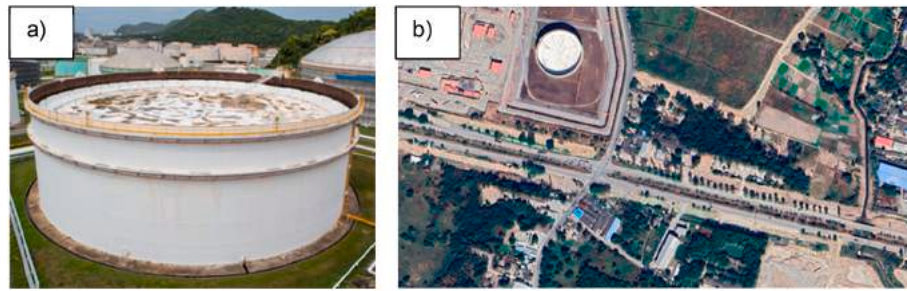
**Fig. 1.** Typical (a) floating storage tank and (b) surroundings of a storage tank in Thailand.

**Table 1**
Class tiles description.

| Class-model | Description | Number of investigated class images | Number of 'other' class associated to the CNN model | Tiles size |
|---|---|---|---|---|
| Floating tank | floating roof tank | 231,403 | 179,851 | 256 × 256 |
| Forest | vegetation and forest | 311,512 | 284,663 | 64 × 64 |
| House | large allotment | 272,604 | 225,514 | 128 × 128 |
| Road | main and secondary roads | 173,856 | 301,111 | 64 × 64 |
| Wasteland | concrete, cement, bare ground | 187,374 | 219,832 | 128 × 128 |
| Water | water and sea water | 214,297 | 300,574 | 64 × 64 |

## 3. Methodology

### 3.1. Overview of land cover processing

The approach proposed by (Fitton et al., 2021) to create the land cover is used in this study and can be summarized as follow.

- CNN models: Building and validation of CNN models associated to each class
- Prediction of each class: The overlapping process proposed by (Chermprayong et al., 2020) is used to reduce the classification area and to improve the land cover on satellite images. An overlapping size of one quarter of the tiles size has been used.
- Post-processing of each predicted class: Predictions are post-processed by removing classified areas that are too small and too large to represent what they are supposed to represent. This given for the studied classes:
  ○ House areas smaller than 2000 m$^2$ are discarded from the model predictions.
  ○ Roads areas smaller and larger than 2250 m$^2$ and 10,000 m$^2$ are respectively removed.
- Land cover aggregation: The assembly of the individual prediction results is performed to obtain the land cover.

### 3.2. Storage tank post-processing methodology

An accurate detection of floating tanks is necessary in order to determine their location and size. A 5-step method is proposed in this work (Fig. 3): CNN prediction; Area Of Interest; Object Detection; Object Reconstruction and Size and density post-processing.

#### 3.2.1. Area Of Interest (AOI)
From the CNN classification (Fig. 3a), a K-means clustering approach

(Lv et al., 2019) is used to detect the different floating tank clusters. For each of these clusters, a square region containing the area is generated named in this work 'Area Of Interest' (Fig. 3b).

#### 3.2.2. Object detection (OD)
As the floating tanks are mainly white while the ground is usually concrete or wasteland, it is possible to summarily extract the tanks. In this study, a RGB filter is applied on each AOI of the associated satellite image (Fig. 3c). The RGB filter has been empirically determined and satellite image pixels having a value higher than 190 on the 3 RGB bands are extracted. Finally, the floating tank prediction given by the associated CNN model is replaced by these pixels (Fig. 3d).

#### 3.2.3. Object Reconstruction (OR)
Due to the OD method based on a RGB filter, extracted floating tanks consists of pixel clouds. Moreover, all features whose colors are within the filter are also extracted. Therefore, it is necessary to rebuild the floating tank and then to remove the false positive identification. Three methods are investigated in this work to obtain the number of clusters, K.

- Elbow Method is used to find the number of the cluster, K, on a dataset through a visual technique (Thorndike, 1953; Syakur et al., 2018; Ketchen and Shook, 1996). Using Sum Square Error calculation, a graphic is obtained and the number of clusters is distinguished by looking at the point position on the "elbow" arm corresponding to the plateau.
- The silhouette method calculates silhouette coefficients of each point measuring how much a point is similar to its own cluster compared to the others (Shutaywi et al., 2021; Suyanto, 2017). The silhouette score is ranged between [1, −1]. A value of 1 indicates that the clustering configuration is appropriate while a low or negative value suggests that the clustering configuration may have too many or too few clusters (Abdullah et al., 2021).

For both of these methods, a range of candidate values of K is picked-up and K-Means clustering is applied for each of these values. As the OD provides a pixel cloud, a value of 40 is chosen in this work.

- Density-Based Spatial Clustering of Applications with Noise algorithm (DBSCAN) is a spatial clustering algorithm based on density (Esterm et al., 1996). Two parameters are required: distance and the minimum sample points (Sander et al., 1998; Schubert et al., 2017). DBSCAN enables the identification of complex cluster shapes and sizes compared to K-Means (Chang et al., 2017). The number of clusters, K, does not need to be known in advance. In this work, a distance of 15 and a number of samples of 5 have been selected empirically in order to limit the consumption of resources.

Finally, knowing the number of clusters, K-means function can be applied to obtain tanks location and size.
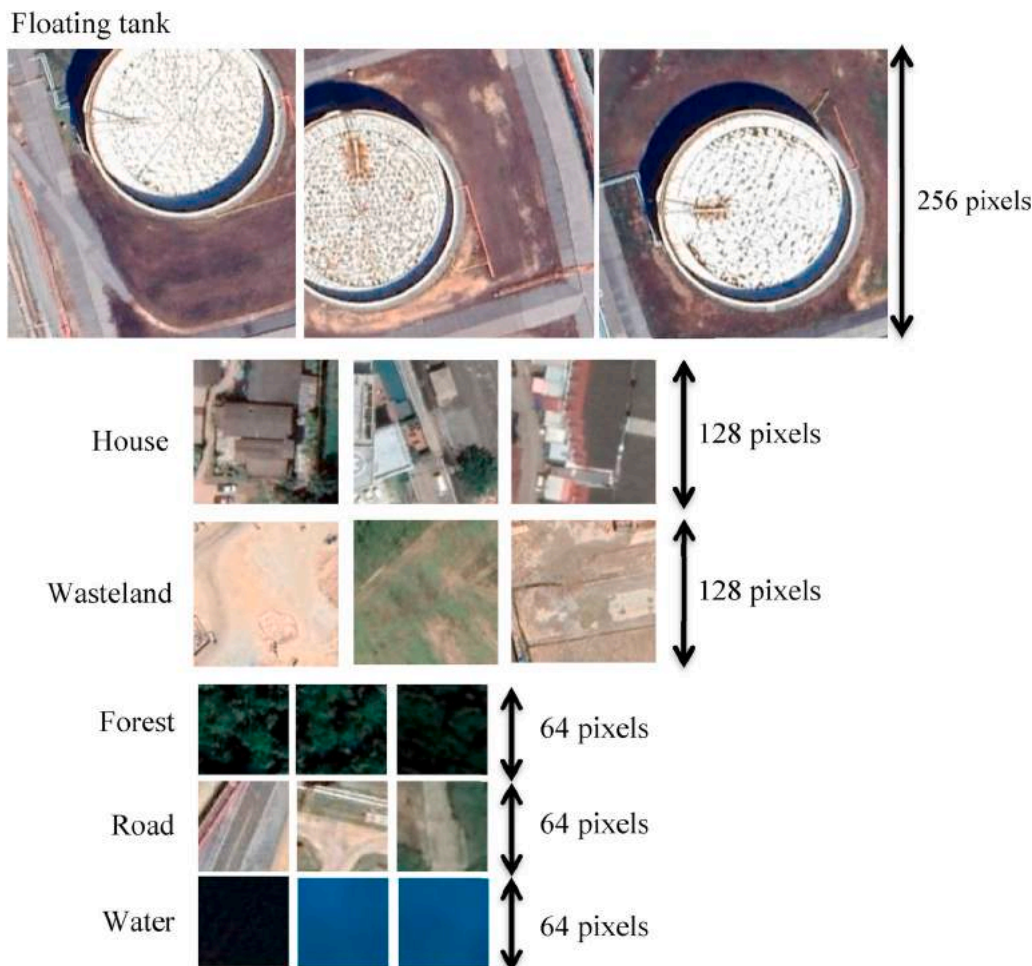
**Fig. 2.** Example of tiles of the different classes used to perform the land cover.

### 3.2.4. Size and density post-processing

A floating tank has standardized sizes even if some rare exception exists (Long and Bob, 2004). Therefore, by using K-means function, it is possible to remove the clusters given by the OR process that are too small and too large to actually be a tank. With a resolution of 0.33m/pixel, clusters having a diameter lower and larger than 25 m and 50 m respectively are removed.

Due to the OR process, based on the clusterization, False Positive features having the same dimensions as a tank can be identified. Therefore, these clusters must be removed and a density-based filter is applied in this study. For each cluster a ratio is calculated that is defined as the sum of the pixels given by the OD step, over the sum of the pixel given by the OR step. To classify as floating tanks, a minimum ratio is set empirically at 30%. Therefore, the label, $L_k$, of each cluster, k, is determined by:

$$L_k = \begin{cases} 0, Ratio_k < 30\% \\ 1, Ratio_k > 30\% \end{cases}$$

where "0" and "1" indicate the "other class" and "floating tank class" class, respectively.

### 3.3. Modeling of explosion

Blast simulation and the estimation of the consequence on peoples, buildings and trees are performed using a 6 steps methodology: TNT charge calculation; blast radius calculation; CNN land cover modification, Effect of the blast on people, Cost estimation and Effect of the blast on trees and road availability. It can be noted that thermal radiation is not investigated in this study.

### 3.3.1. TNT charge calculation

In first step, TNT charge is calculated using 3 sub-steps: estimation of mass of fuel in tank, calculation of the mass of fuel released and calculation of the equivalent mass in TNT charge. Using the floating tank CNN prediction (Fig. 3e), tank diameter can be measured and their volume can be estimated by supposing that their height has a constant value of 14,6 m (International fire code, 2009). Using an average fuel density of 900 kg/m³ (HVVF, 2022), the maximum mass of fuel stored in tanks can be calculated. In order to estimate the quantity of gas created in the cloud before the explosion, the mass of fuel released from the tank due to a leak is needed. It can be obtained by multiplying the mass released from the tank by a coefficient of 2 in order to report the charge in free-air without ground effects (Sochet, 2010). Finally, the mass equivalent of TNT, $W_{TNT}$, can be calculated using (Sochet, 2010):

$$W_{TNT} = \eta_e \frac{w_f \times H_f}{H_{TNT}}$$

where $W_{TNT}$ is the mass equivalent of TNT (kg), $w_f$ is the mass of fuel in the cloud (kg), $H_f$ is the heat of combustion of the fuel (MJ.kg⁻¹), $H_{TNT}$ is the detonation energy of TNT (4.68 MJ kg⁻¹) and $\eta_e$ is the efficiency factor for TNT (0.03).

### 3.3.2. Blast radius calculation

Blast consequences on human, buildings and trees are investigated as

a) Floating tank CNN prediction

b) Area Of Interest

c) Object Detection

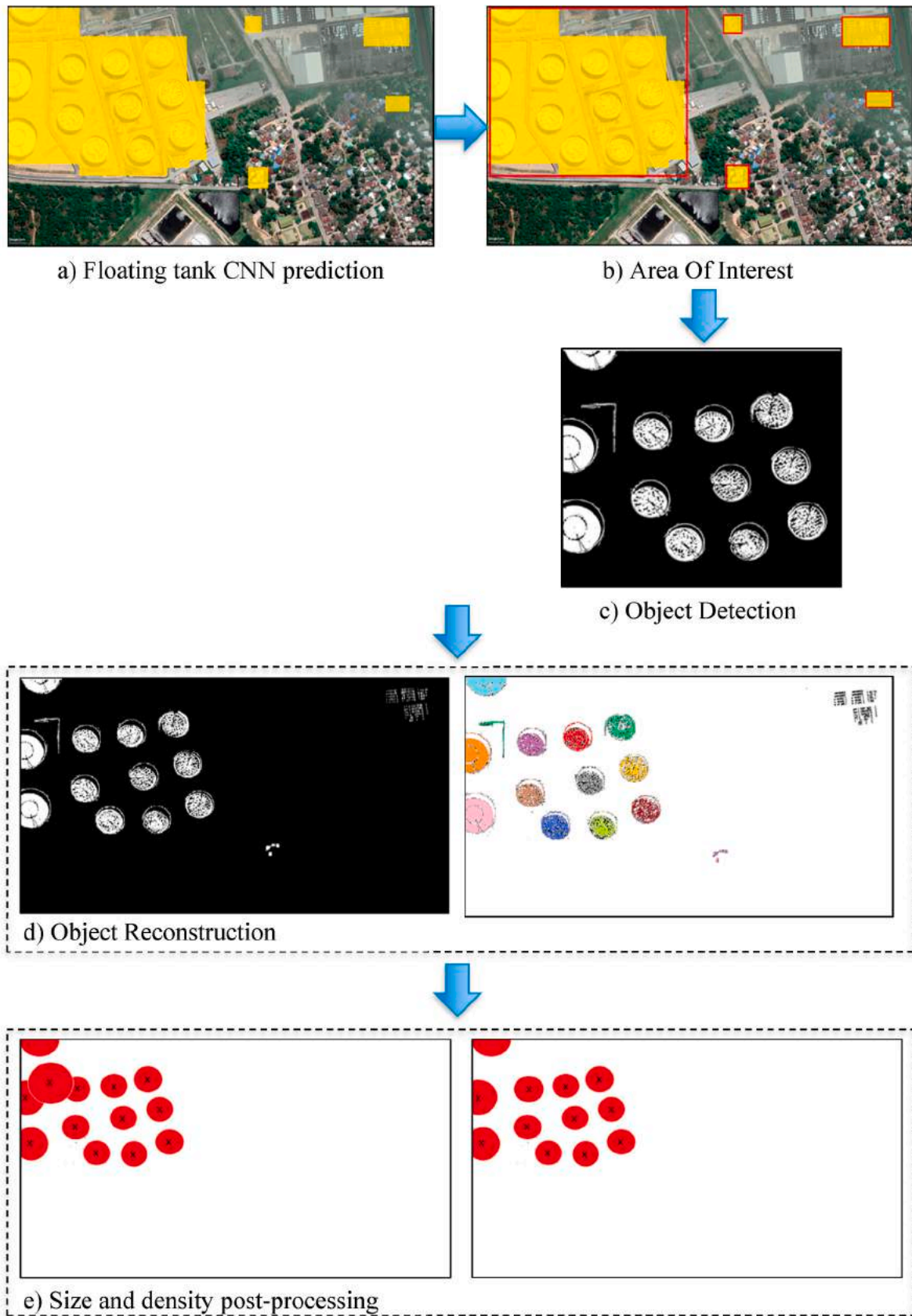d) Object Reconstruction

e) Size and density post-processing

**Fig. 3.** Overall methodology to detect floating storage tanks.

follow.

- Human effects (Alhussan, 2013; Geri, 2016): Minor injuries (bruises, contusions, displacements); injured peoples (fractures, loss of consciousness, internal injuries) and fatalities.
- Structure effects (Alhussan, 2013): Minor damage (windows and doors are forced out); affected structures (severe destruction of least reliable constructions, destruction of residential buildings, severe destruction of buildings made of cast-in-situ reinforced concrete); and structural collapse.
- Tree effects (Fons et al., 1995): Affected trees (fallen tree branches) and fallen trees.

For each of these different effects an overpressure and the associated scaled distance (CPR 1997) are given (Table 2). Finally, the actual distance can be calculated for each scaled distance using the following equation (Sochet, 2010):

$$Actual\ distance = Scaled\ distance \times (W_{TNT})^{1/3}$$

### 3.3.3. CNN land cover modification

In order to visualize and estimate the different blast effects (Table 2), initial class of the land cover are modified. Initial forest and house classes that are within the associated actual distance are modified creating the following sub-classes. On one hand, initial House class is divided into 3 sub-classes related to the structure effects: Minor damage, Affected structure and, Structural collapse classes. On the other hand, 2 sub-classes are created for the Forest class: Affected trees and Fallen trees.

### 3.3.4. Effect of the blast on people

Estimation of the maximum potential human casualty is performed. Only people inside the buildings are considered in this work, pedestrians and workers around the tanks are not investigated. From the land cover the total surface of the different 3 sub-classes House is obtained. Then, the number of houses is estimated by considering an average individual house surface of 150 m$^2$ (Bauer, 2020). The number of people affected by the blast is estimated using an average number of 3.1 people per house (Bauer, 2020). For collapse and affected structures, peoples are considered as death and severely injured respectively while buildings showing minor damage induce light injury.

### 3.3.5. Cost estimation

Damage cost estimation is a crucial information for public authorities and insurance companies. As the number of collapsed and affected houses is determined, damage cost can be estimated. Reconstruction and repair cost of 175,000 and 85,000 Baht per individual house respectively have been used (ADPC, 2014).

### 3.3.6. Effect of the blast on trees and road availability

Fallen trees located near a road have the possibility to block them. A blocked road is a large problem for an emergency as it can slow their progression and in the worst case, prevent them from going further. Therefore, creating a map with a possible blocked road can help the

emergency teams to optimize their path. Moreover, emergency teams can be equipped with the appropriated tools (chainsaw …) in order to open the path. Maximum tree height needs to be estimated in order to know the critical distance between trees and roads that would affect its state. Height depends of the tree species and the climate condition, and a value of 30 m is used (Khamyong et al., 2018). A 3 sub-steps process to identified possible blocked roads is proposed (Fig. 4).

- Clusterization of the fallen trees class: Fallen trees class clusters are identified and following the method proposed by (Fitton et al., 2021), a window is produced around each of them at a specific distance of 30 m (Fig. 4a)
- Road class detection: For each window, road class pixels are identified (Fig. 4b)
- Blocked roads class creation: For each road pixel, a window of 30 × 30 m is created and if a fallen tree pixel is detected, the road class is changed into blocked road class (Fig. 4c).

### 3.3.7. Effect of the blast on surrounding tanks

Storage tanks are usually grouped by creating a farm of tanks (Sirous, 2015). This creates a scenario where the tank explosion can produce a domino effect where surrounding tanks can also explode (Zhang et al., 2019). In this work, storage tanks which are located in the structural collapse area are considered as affected by the blast.

## 4. CNN building and validation

### 4.1. Model construction

The 6 CNN structures, associated with the 6 classes, are based on four conventional layers and one fully connected layer (Fig. 5). As recommended in the literature, all the convolutional layers had 3 × 3 kernels (Mujahidin et al., 2021) and the input image size depended on the class tiles size. To avoid overfitting, four max pooling operations are applied after each convolutional layer with a pooling rate of 0.4. A drop-out layer has been used only after the dense layer and a softmax activation is used after the output layer (Fig. 5). Rectified Linear Unit (ReLU) and local response normalization are used as transfer functions after all convolutional and dense layers. A L2 penalty multiplier (0.01) is set only after the dense layer. The training of the model is affected by the batch size that is one of the hyperparameters and has been optimized. The network has been trained under the Windows environment using Python 3.9.12 and Tensorflow 2.9.1 and on a computer with an Intel i5 processor 12th Gen with 3.3 GHz and 12 GB of RAM. Different configurations for the size of each layer have been tested and the one provided the best results has been chosen. Models to classify floating tanks class requires 16 nodes for both convolutional and the fully connected layer while the others classes need 32 nodes. A batch size of 256 samples has been used for all the classes and the model parameters have been optimized using RMSPROP with a fixed learning rate of 0.0001. To avoid the overfitting the model was trained using an early stopping approach with a patience of 50 consecutive epochs. The final weights are those that provided the best overall validation accuracy.

### 4.2. CNN validation

To evaluate detection performance accuracy is commonly used (Olson and Delen, 2008):

$$Accuracy = \frac{TP}{TP + TN + FP + FN}$$

where TP and FP are respectively True Positive and False Positive. FN is False Negative while TN is True Negative. The confusion matrix provides an overview of both accuracy (Fig. 6). The accuracy of the CNN models for floating tank, forest, house and water is higher than 96%. Wasteland
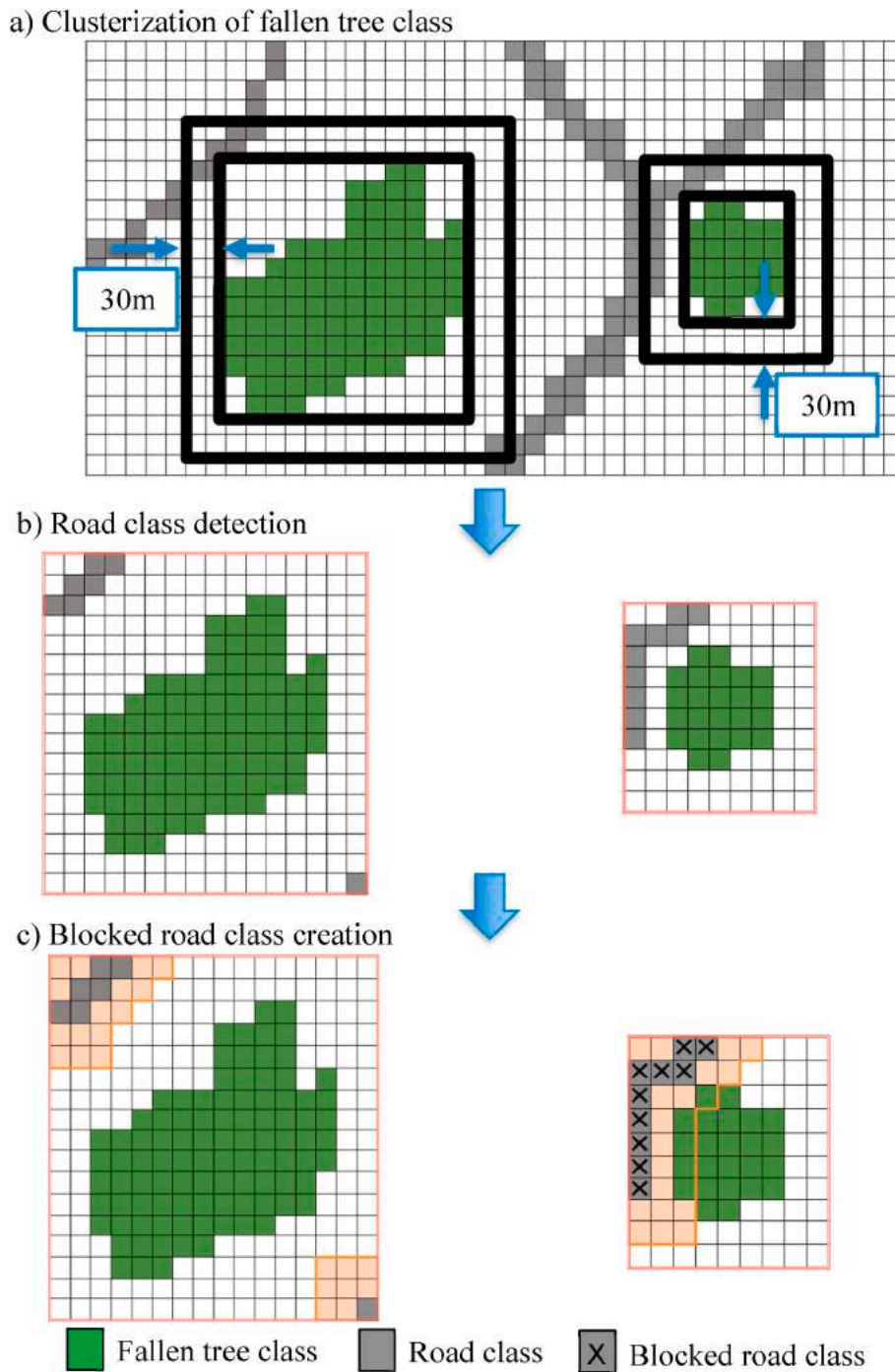
**Table 2**
Blast consequence and associated scaled distance.

| Human effects | Structure effects | Tree effects | Overpressure | Scaled distance (m/kg$^3$) |
|---|---|---|---|---|
| Fatalities | Structural collapse | Fallen Trees | 8.00 bar | 1.1 |
|  |  |  | 2.00 bar | 2.3 |
|  | Affected structures | Affected trees | 0.50 bar | 5.0 |
| Injured peoples |  |  | 0.07 bar | 18.0 |
| Minor injuries | Minor damage |  | 0.03 bar | 33.0 |

**Fig. 4.** Effect of damaged trees on road availability process.

CNN model shows an intermediate accuracy of 88.9% while the road model has the lowest accuracy (73.4%). This low precision can be related to the low number of tiles (Table 1) as detailed by (Ruiz Emparanza et al., 2020; Chermprayong et al., 2020).

## 5. Results

### 5.1. Individual class model's prediction

Land cover has been performed at the petrochemical facilities of LaemChabang, having 15 floating tanks and representing an area of 0.8 km$^2$ with a resolution of 0.33 m/pixel (Fig. 7a). The prediction results of the house class (Fig. 7b), forest (Fig. 7c) wasteland (Fig. 7d), water

(Fig. 7e), road (Fig. 7f), and floating tank (Fig. 7g) are shown in the respective Figures. The house CNN model can identify most of the houses except some large buildings. It can be noted that the sea border and some complex industrial facilities are classified under this class. Forest class is very well identified except that the CNN model also classified the water. The beach and some areas around tanks are identified as wasteland but grass is not classified. Water class is well detected. Due to the occlusion from trees and buildings roads are partially detected (Fig. 7f). It can be observed that the roads around the tanks are difficult to classify due to the industrial features, such pipes, along it. Finally, the floating tanks farm is classified under the right class but some False Positive classification are also observed.
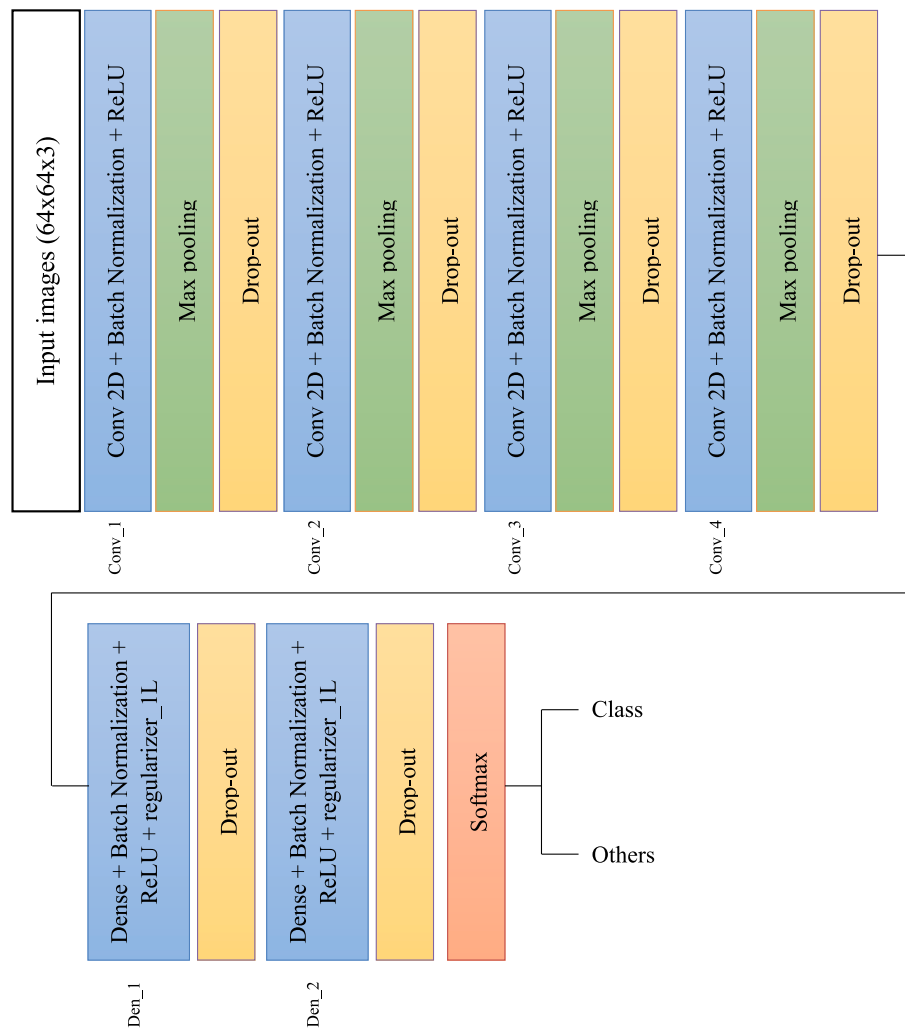
**Fig. 5.** Flow chart of the Convolutional Neural Network architecture.

### 5.2. Floating tank post-processing

Object Detection methodology to obtain the tanks are applied on the associated CNN results (Fig. 3c). In first step, using RGB filters on the AOI tanks can be highlighted (Fig. 8). Due to the initial CNN prediction, some other types of tank are also extracted. Moreover, the RGB filter also extracts buildings having a white roof.

In the second step, clustering using Elbow, Silhouette score and DBSCAN methods is performed in order to determine the appropriate method to find the number of clusters (Fig. 3d). Following the Elbow method, six clusters are determined (Fig. 9a), that are lower than the 15 floating tanks observed in Fig. 7a. Silhouette score provides a better result than the Elbow method with 18 identified clusters. However, this method is time consuming with a total of 24 h to perform the analysis (Fig. 9b). Finally, it can be noted that this method can be applied only for at least 2 clusters, limiting its use. DBSCAN results show a computing time of about 7s that is largely faster than the 2 others methods. As observed, 33 clusters are identified that are largely higher than the number of floating tanks (Fig. 9c).

DBSCAN provides a fast and effective way to detect at least the tanks. Therefore, it is necessary to remove the False Positive clusters. In last step, size and density post-processing are applied in order to remove it (Fig. 3e). Utility of the density post-processing is given through an example in Fig. 10. As observed, True Positive tank is well identified while the False Positive (in this case a pipe) can be removed from the

classification. By applying these 2 post-processing, floating tank prediction can be obtained (Fig. 11). It can be noted that one floating tank is removed from the classification due to the density post processing parameter.

### 5.3. Land cover

CNN results are aggregated in order to perform the land cover of the studied area (Fig. 12a). The chosen approach to determine the class of each pixel is to select the class having the highest accuracy amongst the individual CNN models. Forest and water classes are well identified. Buildings show a good classification, excepted near the storage tanks where False Positive classification is observed. Indeed, reservoir is detected as House class. A lot of wasteland areas and roads are not detected especially inside the industrial facilities and forest. Finally, the areas where no class has been identified are displayed in gray and correspond to mainly undetected roads, wasteland and other tanks types (Fig. 12b), and are identified under 'Unclassified' class.

### 5.4. Blast consequence analysis

An explosion of the closest storage tank from the buildings is investigated (Fig. 13). As a typical storage tank explosion creates a blast at 340 m, an equivalent TNT kg of 1200 tons is used. The 3 storage tanks near the center of the explosion are potentially damaged or destroyed
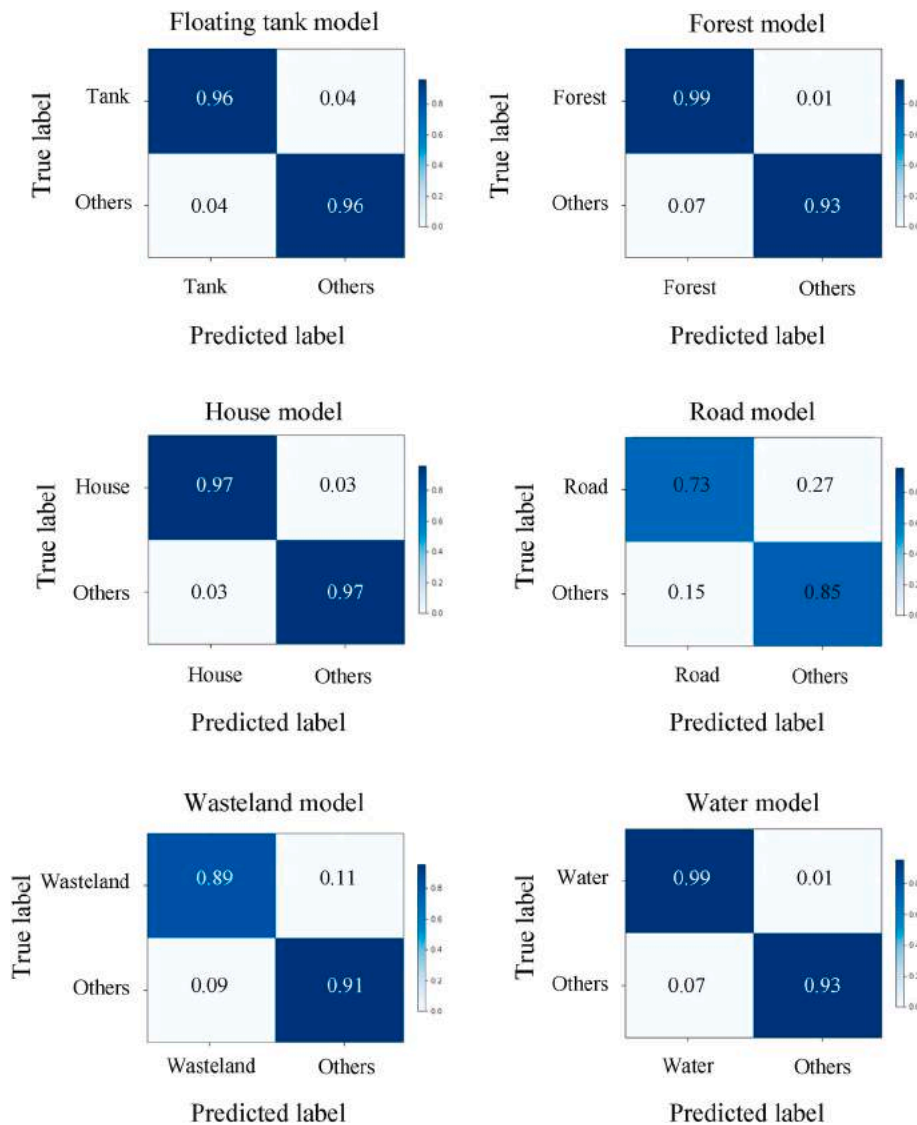
Fig. 6. Confusion matrix for each of the 6 CNN models.

(Fig. 13). Using the proposed method, surface of damaged buildings and trees are obtained. The 3 sub-class related to the damage effects can be identified and displayed in Fig. 13. It can be noted that all buildings in the studied area show a potential effect. As few houses are built near the petrochemical facilities, collapsed houses are limited (8,350 m$^2$) for a destruction cost of 225,700 US dollars. However, due to false positive classification of house near the tank (Fig. 12b), this number is therefore overestimated. Buildings which are a little further, within a range of a blast pressure of 0.07–0.5 bars, show a severe destruction for a surface of 20,000 m$^2$. All the other buildings can be potentially affected by the blast given an area of light damage of 300,000 m$^2$. Number of potential casualties (173), severe (414) and light (6,180) injuries are estimated. As it is related to the surface of the collapsed house, the maximum potential number of fatalities is overestimated. Fallen and affected trees surface is given with a surface of 13,430 m$^2$ and 52,000 m$^2$ respectively. Using the method (Fig. 4), potential blocked roads are displayed (Fig. 13).

## 6. Discussion

### 6.1. Limitation

CNN models show limitations especially in the detection for

wasteland and roads classes. Lands around industrial storage tanks are not classified as wasteland (Fig. 1b). Indeed, these area shows a complex feature with a mix of grass, concrete, road, pipes that is not included into the Wasteland dataset. Dataset improvement would enable to detect these areas. Moreover, a tile size of 128 × 128 pixels has been selected (Table 1) that is larger than areas between tanks, and therefore, decreasing the tiles size could help to classify. However, decreasing the size of tiles has an effect on the classification as the context of the class will be reduced and therefore could be difficult to predict (Mezeix and Casanova, 2022). As observed, some types of land such as the beach and grassland are not classified as Wasteland class. A lack of land diversity in the dataset explains the result of the associated CNN model. Therefore, a larger dataset with more representative land type should be built. However, to be able to classify such features, data will need to be collected to create the dataset, which can be challenging.

Roads are partially detected only when there is no occlusion (Fig. 7f). As explained in the literature, it is difficult to extract roads from remote sensing images due to occlusions by trees, buildings and large shadows cast by buildings (Mattyus et al., 2017). Overlapping of 16 pixels (5 m) has been used in this study and therefore the road class detection is limited (Fig. 14a). The classification can be improved by reducing the overlapping value, but computing costs will increase (Fig. 14b). Different solutions have been successfully proposed in the literature to
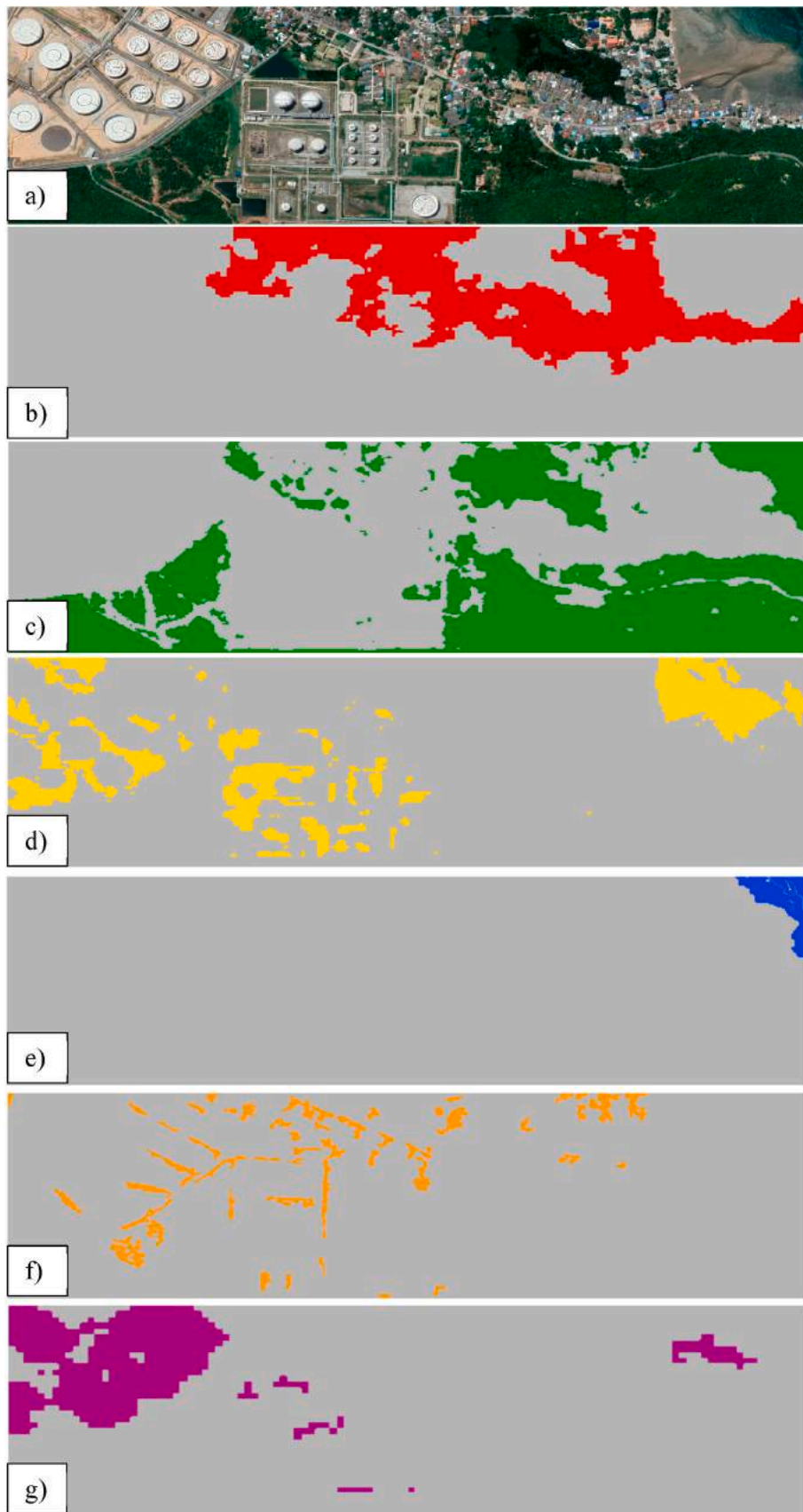
**Fig. 7.** (a) Investigated satellite image. Prediction given by CNN models for (b) building, (c) forest and (d) wasteland, (e) water, (f) road and (g) floating tank (color shows the associated class). (For interpretation of the references to color in this figure legend, the reader is referred to the Web version of this article.)

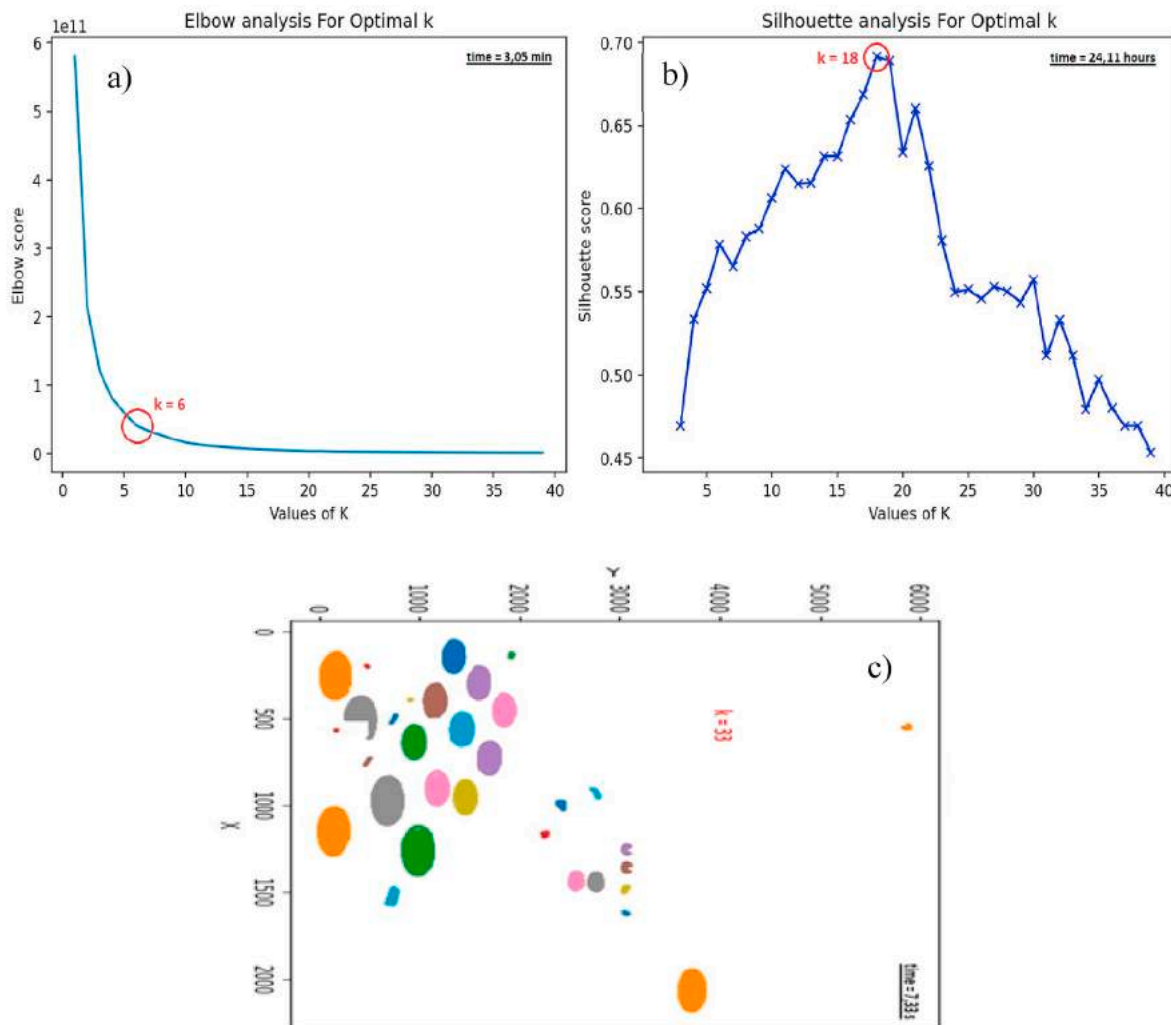**Fig. 8.** Tank detection using RGB filter.



**Fig. 9.** Results of (a) Elbow, (b) Silhouette and (c) DBSCAN methods.

detect roads: combination of different models (Choudhury et al., 2020), use of Lidar data (Parajuli et al., 2018) and Object-oriented classification approach (Mhangara et al., 2011). However, both of these two approaches are complex and computationally expensive.

In this study, blast has been simulated and fatalities/injuries number has been estimated from the damaged/collapsed building. As House class has shown False Positive classification, fatalities number has been overestimated. In the same way Wasteland and Road class can be improved, increasing the size of dataset and adding more diversity will enable to obtain a better House class prediction. Finally, thermal radiation can impact peoples depending of the radiation level flux (Bariha

et al., 2016). That can be simulated (Robert, 1981) using the proposed method and to estimate the different effects (Bhisham et al., 2015).

### 6.2. Perspective

CNN land cover enables to detect wasteland areas which are the zones either without vegetation nor construction. Therefore, it would be possible to detect potential areas where emergency base camps could be installed in order to rescue injured people. Different condition can be applied as a minimal area (The UN Refugees Agency, 2022) or area closes to buildings and roads for running water and electricity access.
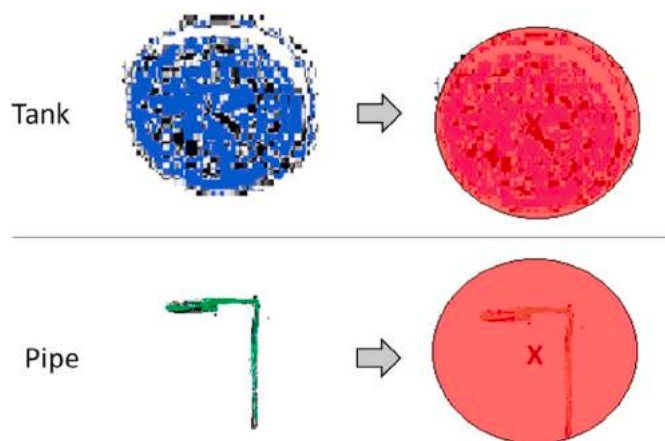
**Fig. 10.** Example of density post-processing.

Proposed method can be also used for other types of storage tank as liquefied natural gas (Zhu et al., 2021) or spherical storage tanks (Zhang and Wang, 2015).

Risk is defined as a measure of human casualty, environmental damage and economic loss in terms of the probability of incident and its effects (Center for Chemical Process Safety, 2000). It is usually described in terms of 2 concepts: individual and societal risk (Ale, 1993; Ale, 2002; Bottelberghs, 2000; Renjith and Madhu, 2010). The risk estimation requires gathering and integrating information about various scenarios, in particular looking at likelihood and consequences of these scenarios. Risk analysis and risk map have been performed manually for the storage tanks located at the Izmit Bat in Turkey (Girgin and Krausmann, 2013). Hand operation is time consuming and inaccurate data/information can be used/extracted. By combining the frequency and probability of incident with the data given by the method presented in this paper, accurate risks and risk map can be calculated and proposed to the safety policy maker.

## 7. Conclusions

Gas, oil, and petrochemical products employed for oil and petrochemical industries are stored into industrial storage tanks. Fire and explosion accidents due to flammable materials can create blast waves and thermal radiation causing casualties, infrastructure damages, pollution to the environment and economic losses. In order to establish the right emergency response and to facilitate it, two critical information must be obtained. Firstly, to be able to detect automatically storage tanks and the surrounding environment and, secondly to determine and visualize the effect/consequence of a tank explosion. In this work, data



**Fig. 11.** Floating tanks prediction after processing.



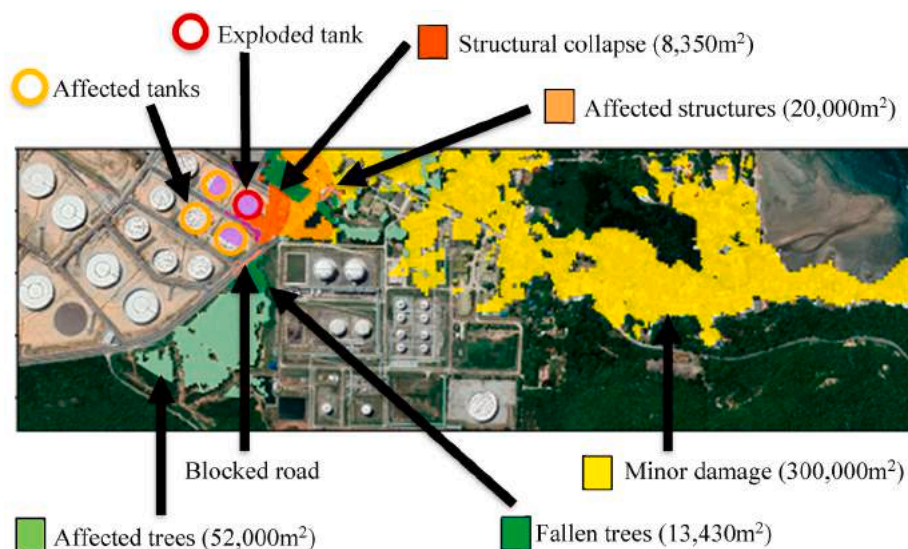**Fig. 12.** (a) Satellite image and (b) land cover and of the petrochemical facilities of LaemChabang.

**Fig. 13.** Potential blast effects around petrochemical facilities of LaemChabang.
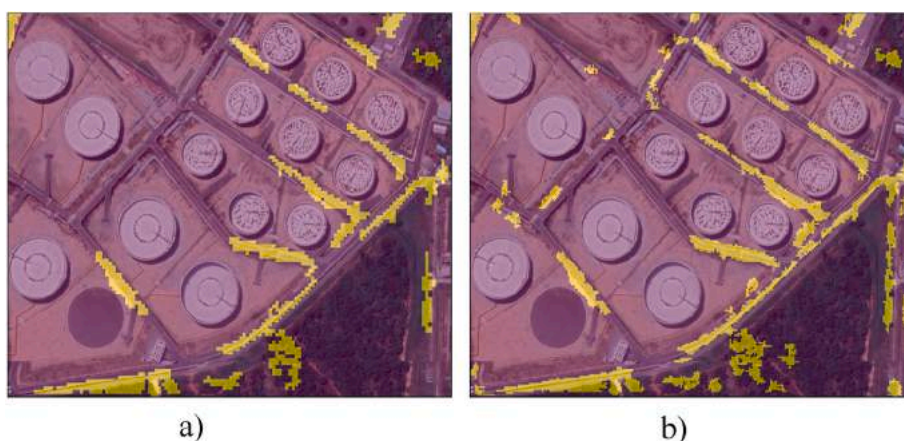


**Fig. 14.** Effect of overlapping size on the road classification, (a) 16 pixels and (b) 8 pixels (yellow color = road class). (For interpretation of the references to color in this figure legend, the reader is referred to the Web version of this article.)

obtained from a land cover, performed by CNN models, are used as input of blast model/simulation enabling automatically the estimation of human casualties/injuries and of damaged buildings. The advantage of the proposed method is to be able to provide all information required by the authorities from only 1 data source.

First, to perform it, 6 classes dataset are built: floating storage tank, forest, house, road, wasteland and water for a total number of tiles of about 1.4 million. Satellite images with a resolution of 0.33 m/pixel are used. Tiles size has been optimized for each class. Floating tank requires tiles of 256 × 256 pixels in order to have enough contact to be classified. House and wasteland need a size of 128 × 128 pixels while the others classes need smaller tiles (64 × 64 pixels). Then, each CNN model associated with each class is developed, optimized and validated. Results show an accuracy higher than 96% for house, forest, floating tank and water. Due to the small size of the dataset, wasteland and roads have low accuracy with a value of 88.9% and 73.4% respectively. The proposed method using DBSCAN to post-process the floating tank detection shows its effectiveness to precisely obtain their size and location. The land cover is achieved by aggregating the different predictions. Unclassified areas are mainly roads, large buildings and some wasteland as grassland. In order to improve the land cover, the wasteland dataset must be upgraded by adding a larger diversity of land. By reducing the overlapping, roads detection can be improved but computing resources

will significantly increase. Secondly, blast simulation is performed based and the overpressure created by the explosion. Different types of effects are investigated: human, building and trees. Building and trees class are modified on the CNN in order to be able to displayed these effects. From the type of building damage, human casualties/injuries are estimated. Potential roads blocked by fallen trees are given by the method and display on the remote sensing image. From the case study of Laem-Chabang petrochemical facility, the tool shows efficiency to help the emergency to plan the response.

**Credit author statement**

T. Sentagne Coding; experimentation; Writing – original draft. M. Zerbola Coding; experimentation; Writing – original draft. M. Garcia Coding; experimentation; Writing – original draft. C. Kumsap Methodology, experimentation. V. Mungkung Methodology, experimentation. L. Mezeix Software; Methodology; Supervision; Writing – original draft.

**Declaration of competing interest**

The authors declare that they have no known competing financial interests or personal relationships that could have appeared to influence the work reported in this paper.

## Data availability

Data will be made available on request.

## References

Abdullah, A.I., Priadana, A., Muhajir, M., Nur, S.N., 2021. Data mining for determining the best cluster of student instagram account as new student admission influencer. Telematika: Jurnal Informatika dan Teknologi Informasi 18, 255–266.

Ale, B.J.M., 1993. Dealing with risks of fixed installations in The Netherlands. Cryogenics 33, 762–766.

Ale, B.J.M., 2002. Risk assessment practices in The Netherlands. Saf. Sci. 40, 105–126.

Alhussan, K., 2013. Thermal radiation of explosion: estimations of risk of thermal defeat of people and occurrence of fires. Procedia Eng. 61, 185–191.

Anjana, N.S., Amarnath, A., Chithra, S.V., Harindranathan Nair, M.V., Subin Jose, K., 2015. Population vulnerability assessment around a LPG storage and distribution facility near Cochin using ALOHA and GIS. Int. J. Eng. Sci. Invent. 4, 23–31.

Anjana, N.S., Amarnath, A., Harindranathan Nair, M.V., 2018. Toxic hazards of ammonia release and population vulnerability assessment using geographical information system. J. Environ. Manag. 210, 201–209.

Asian Disaster Preparedness Center (ADPC), 2014. The Economic Impact of the 26 December 2004 Earthquake and Indian Ocean Tsunami in Thailand.

Awrangjeb, M., Lu, G., 2008. Robust image corner detection based on the chord-to-point distance accumulation technique. IEEE Trans. Multimed. 10, 1059–1072.

Bariha, N., Mishra, I.M., Srivastava, V.C., 2016. Fire and explosion hazard analysis during surface transport of liquefied petroleum gas (LPG): a case study of LPG truck tanker accident in Kannur, Kerala, India. J. Loss Prev. Process. Ind. 40, 449–460.

Basu, S., Ganguly, S., Mukhopadhyay, S., DiBiano, R., Karki, M., Nemani, R., 2015. Deepsat: a learning framework for satellite imagery. In: Proc. 23rd SIGSPATIAL International Conference on Advances in Geographic Information Systems, vol. 37, 3-6 November.

Bauer, D., 2020. Average household size in Thailand. In: Esri Demographics.

Bhisham, K., Dhurandher, Ravi Kumar, Amit, Dhiman, 2015. Impact assessment of thermal radiation hazard from LPG fireball. Procedia Earth. Planet. Sci 11, 499–506.

Bhosle, K., Musande, V., 2019. Evaluation of deep learning CNN model for land use land cover classification and crop identification using hyperspectral remote sensing images. J. Indian Soc. Rem. Sens. 47, 1949–1958.

Bottelberghs, P.H., 2000. Risk analysis and safety policy developments in The Netherlands. J. Hazard Mater. 71, 117–123.

Cai, X., Sui, H., Ruipeng, L.V., Song, Z., 2014. Automatic circular oil tank detection in high-resolution optical image based on visual saliency and hough transform. In: Electronics, Computer and Applications, IEEE Workshop on. IEEE, Ottawa, ON, Canada, pp. 408–411.

Center for Chemical Process Safety (CCPS), 2000. Guidelines for Chemical Process Quantitative Risk Analysis, second ed. Center for Chemical Process Safety, American Institute of Chemical Engineers (AIChE), New York.

Chang, D., Ma, Y., Ding, X., 2017. Time series clustering based on singularity. Int. J. Comput. Commun. Control 12, 790.

Chem, E., 2008. BP Process Safety Series, Liquid Hydrocarbon Tank Fires: Prevention and Response, fourth ed. U.K.

Cheng, L., Li, S., Ma, L., Li, M., Ma, X., 2015. Fire spread simulation using GIS: aiming at urban natural gas pipeline. Saf. Sci. 75, 23–35.

Cheolhee, Y., Daehyeon, H., Jungho, I., Benjamin, B., 2019. Comparison between convolutional neural networks and random forest for local climate zone classification in mega urban areas using Landsat images. ISPRS J. Photogrammetry Remote Sens. 157, 155–170.

Chermprayong, P., Hongkarnjanakul, N., Rouquette, D., Schwob, C., Mezeix, L., 2020. Convolutional neural network for Thailand's Eastern Economic Corridor (EEC) land cover classification using overlapping process on satellite images. Remote Sens. Appl.: Soc. Environ. 20, 100543.

Choudhury, R.A., Biswas, P., Piyush, K., 2020. QuadRoad: an ensemble of CNNs for road segmentation. Procedia Comput. Sci. 176, 138–147.

Cihan, M., Ceylan, M., Soylu, H., Konak, M., 2021. Fast Evaluation of Unhealthy and Healthy Neonates Using Hyperspectral Features on 700-850 Nm Wavelengths, ROI Extraction, and 3D-CNN. IRBM. Available online 5 July 2021.

CPR, 1997. Committee for the Prevention of Disaster, Yellow Book, Methods for the Calculation of Physical Effects, Part 2, CPR 14E, third ed. Chap. 5.

Elmaz, F., Eyckerman, R., Casteels, W., Latré, S., Hellinckx, P., 2021. CNN-LSTM architecture for predictive indoor temperature modeling. Build. Environ. 206, 108327.

Enterprise Security Assistant, 2019. Nationwide Compilation of Typical Accident Cases of Chemical and Hazardous Chemicals. https://www.sohu.com. (Accessed 26 February 2019). Accessed.

Esterm, M., Kriegelm, H.P., Xum, X., 1996. A density-based algorithm for discovering clusters a density-based algorithm for discovering clusters in large spatial databases with noise. Int. Conf. Knowl. 226–231.

European Council, 1982. Council directive 82/501/EEC on the major accident hazards of certain industrial activities (SEVESO I). Off. J. Eur. Communities - Legislation. 1–48.

Fernanda, S.Y.W., Gabriela, T.M., Thanan, W.P.R., Nariane, M.R.B., Luiz, H.S.R., Enner, A., Nilton, N.I., 2020. Inland water's trophic status classification based on machine learning and remote sensing data. Remote Sens. Appl.: Soc. Environ. 19, 100326.

Fitton, D., Laurens, E., Hongkarnjanakul, N., Schwob, C., Mezeix, L. Land cover classification through Convolutional Neural Network model assembly: a case study of a local rural area in Thailand. Remote Sens. Appl.: Soc. Environ., 26, 100740.

Fons, W.L., Storey, T.G., 1995. Operation Castle. Project 3.3. Blast Effects on Tree Stand. Unclassified Report. U.S. Department of Agriculture, Forest Service, Division of Fire Research.

Geri, F., 2016. Scenarios and Evaluation of the Effects of Explosive Mixtures. Prevention and Protection Methods. National department of Civil protection - Technological risk, Italy.

Girgin, S., Krausmann, E., 2013. Case Study Application of RAPID-N. European Commission. Joint Research Centre.

Huang, X., Zhang, L., 2013. An SVM ensemble approach combining spectral, structural, and semantic features for the classification of high-resolution remotely sensed imagery. IEEE Trans. Geosci. Rem. Sens. 51, 257–272.

HVVF, 2022. Heat Values of Various Fuels. https://chemeng.queensu.ca/courses/CHEE332/files/ethanol_heating-values.pdf.

International fire code, 2009. Chapter 34: Flammable and Combustible Liquids, Article 3406.4.5.3: Height of Aboveground Storage Tanks.

Jean-Daniel, S., Guillaume, D., Nicolas, B., 2019. Mapping dead forest cover using a deep convolutional neural network and digital aerial photography. ISPRS J. Photogrammetry Remote Sens. 156, 14–26.

Jivane, N.J., Rajkumar, S., 2017. Enhancement of an algorithm for oil tank detection in satellite images. Int. J. Intell. Eng. Syst. 10, 218–225.

Kanghui, Z., Weidong, W., Ziqi, L., Yuhan, F., Yang, S., 2021. Computer vision detection of foreign objects in coal processing using attention CNN. Eng. Appl. Artif. Intell. 102, 104242.

Ketchen, D.J., Shook, C.L., 1996. The application of cluster analysis in strategic management research: an analysis and critique. Strat. Manag. J. 17, 441–458.

Khamyong, N., Wangpakapattanawong, P., Chairuangsri, S., Inta, A., Tiansawat, P., 2018. Tree species composition and height-diameter allometry of three forest types in northern Thailand. Chiang Mai Univ. J. Nat.Sci.

Khanmohamadi, M., Bagheri, M., Khadem, N., Ghannadpour, S.F., 2018. A security vulnerability analysis model for dangerous goods transportation by rail – case study: chlorine transportation in Texas-Illinois. Saf. Sci. 110, 230–241.

Knegtering, B., Pasman, H.J., 2009. Safety of the process industries in the 21st century: a changing need of process safety management for a changing industry. J. Loss Prev. Process. Ind. 22, 162–168.

Kushwaha, N.K., Chaudhuri, D., Singh, M.P., 2013. Automatic bright circular type oil tank detection using remote sensing images. Defence Sci. J. 63, 298–304.

Li, Q., Chen, Y., Zeng, Y., 2022. Transformer with transfer CNN for remote-sensing-image object detection. Rem. Sens. 14, 984.

Li, W., Chen, C., Zhang, M.M., Li, H.C., Du, Q., 2019. Data augmentation for hyperspectral image classification with deep CNN. Geosci. Rem. Sens. Lett. IEEE 16, 593–597.

Li, Z., Itti, L., 2011. Saliency and gist features for target detection in satellite images. IEEE Trans. Image Process. 20, 2017–2029.

Li, Z., Wu, L., 2019. Efficient object detection framework and hardware architecture for remote sensing images. Rem. Sens. 11, 2376.

Loh, R., Yong, W.X., Yapeter, J., Subburaj, K., Chandramohanadas, R., 2021. A deep learning approach to the screening of malaria infection: automated and rapid cell counting, object detection and instance segmentation using Mask R-CNN. Computerized medical imaging and graphics. Mining. Knowl. Discov 88, 101845.

Long, B., Bob, G., 2004. Guide to Storage Tanks & Equipment. Professional Engineering, Bury St. Edmunds. U.K., 2004.

Lu, C., Yang, X.M., Wang, Z.H., Li, Z., 2018. Using multi-level fusion of local features for land-use scene classification with high spatial resolution images in urban coastal zones. Int. J. Appl. Earth Obs. Geoinf. 70, 1–12.

Lucyna, B., 2016. Computer simulation of impacts of a chlorine tanker truck accident. Transport. Res. Transport Environ. 4, 107–122.

Lv, Z., Liu, T., Benediktsson, J., Du, H., 2019. A novel land cover change detection method based on K-means clustering and adaptive majority voting using bitemporal remote sensing images. IEEE Access 7, 34425–34437.

Ma, L., Cheng, L., Li, M., 2013. Quantitative risk analysis of urban natural gas pipeline networks using geographical information systems. J. Loss Prev. Process. Ind. 26, 1183–1192.

Ma, L., Liu, Y., Zhang, X., Ye, Y., Yin, G., Johnson, B.A., 2019. Deep learning in remote sensing applications: a meta-analysis and review. ISPRS J. Photogrammetry Remote Sens. 152, 166–177.

Mahdi, P., Nitheshnirmal, S., Hamid, R.P., Fatemeh, R., Saro, L., 2020. Spatial prediction of groundwater potential mapping based on convolutional neural network (CNN) and support vector regression (SVR). J. Hydrol. 588, 125033.

Mattyus, G., Luo, W., Urtasun, R., 2017. DeepRoadMapper: Extracting Road Topology from Aerial Images, pp. 3458–3466.

Mentet, M., Hongkarnjanakul, N., Schwob, C., Mezeix, L., 2022. Method to apply and visualize physical models associated to a land cover performed by CNN: a case study of vegetation and water cooling effect in Bangkok Thailand. Remote Sens. Appl.: Soc. Environ. 28, 100856.

Mezeix, L., Casanova, M.G., 2022. Dataset creation methodology for CNN land use/cover classification: Thailand's rural area study case. Def. Techn. Acad. J 3.

Mhangara, P., Odindi, J., Kleyn, L., Remas, H., 2011. Road Extraction Using Object Oriented Classification. Visualisation technical.

Mnih, V., Hinton, G.E., 2010. Learning to detect roads in high-resolution aerial images. In: Proceedings of the 11th European Conference on Computer Vision (ECCV). 5-11 September.

Moein, Z., Gholamreza, A., Navid, A.S., 2019. A new approach for oil tank detection using deep learning features with control false alarm rate in high-resolution satellite imagery. Int. J. Rem. Sens. 41, 2239–2262.

Mujahidin, S., Azhar, N.F., Prihasto, B., 2021. Analysis of using regularization technique in the convolutional neural network architecture to detect paddy disease for small dataset. In: Journal of Physics: Conference Series, vol. 1726. Energy Transition, Smart Technology and Global Environment for Sustainable Development (BICAME III) 2020 9-10 September 2020, Balikpapan, Indonesia.

Nilambar, B., Indra, M.M., Vimal, C.S., 2016. Fire and explosion hazard analysis during surface transport of liquid petroleum gas (LPG): a case study of LPG truck tanker accident in Kannur, Kerala, India. J. Loss Prev. Process. Ind. 40, 449–460.

Ok, A.O., 2014. A new approach for the extraction of aboveground circular structures from near-nadir VHR satellite imagery. IEEE Trans. Geosci. Rem. Sens. 52, 3125–3140.

Ok, A.O., Emre, B., 2015. Circular oil tank detection from panchromatic satellite images: a new automated approach. Geosci. Rem. Sens. Lett. IEEE 12, 1347–1351.

Olson, D., Delen, D., 2008. Advanced Data Mining Techniques. Springer, Publisher.

Parajuli, B., Kumar, P., Mukherjee, T., Pasiliao, E., Jambawalikar, S., 2018. Fusion of aerial lidar and images for road segmentation with deep CNN. In: Proceedings of the 26th ACM SIGSPATIAL International Conference, pp. 548–551.

Rahman, N., Ansary, M.A., Islam, I., 2015. GIS based mapping of vulnerability to earthquake and fire hazard in Dhaka city, Bangladesh. Int. J. Disaster Risk Reduc. 13, 291–300.

Rajeev, K., Soman, S., Renjith, V.R., George, P., 2019. Human vulnerability mapping of chemical accidents in major industrial units in Kerala, India for better disaster mitigation. Int. J. Disaster Risk Reduc. 39, 101247.

Recycling Business Network, 2017. 31 Typical Cases of Global Factory Explosion and Leakage Accidents in 2016 Ring Alarm. http://news.huishoushang.com/81589.html. (Accessed 15 July 2022). Accessed.

Renjith, V.R., Madhu, G., 2010. Individual and societal risk analysis and mapping of human vulnerability to chemical accidents in the vicinity of an industrial area. Int. J. Appl. Eng. Res. 1, 135–148.

Robert, A., 1981. Thermal radiation hazards from release of LPG pressurized storage. Fire Saf. J. 40, 197–212.

Ruiz Emparanza, P., Hongkarnjanakul, N., Rouquette, D., Schwob, C., Mezeix, L., 2020. Land cover classification in Thailand's Eastern Economic Corridor (EEC) using convolutional neural network on satellite images. Remote Sens. Appl.: Soc. Environ. 20, 100394.

Sander, J., Ester, M., Kriegel, H.-P., Xu, X., 1998. Density-based clustering in spatial databases: the algorithm GDBSCAN and its applications. Min. Knowl. Discov 2, 169–194.

Schubert, E., Sander, J., Ester, M., Kriege, H.P., Xu, X., 2017. DBSCAN revisited, revisited: why and how you should (still) use DBSCAN. ACM Trans. Database Syst. 42, 19:1–19:21.

Shutaywi, M., Kachouie, N., 2021. Silhouette analysis for performance evaluation in machine learning with applications to clustering. Entropy 23, 759.

Sirous, Y., 2015. Blast pressure distribution around large storage tanks. Fabig Newsletter Published by Steel Construction Institute UK 67, 22–30.

Sochet, I., 2010. Blast effects of external explosions. In: Eighth International Symposium on Hazards, Prevention, and Mitigation of Industrial Explosions. Yokohama, Japan. hal-00629253.

Suyanto, 2017. Data Mining Untuk Klasifikasi Dan Klasterisasi Data. Bandung: Informatika.

Syakur, M.A., Khotimah, B.K., Rochman, E.M.S., Satoto, B.D., 2018. Integration K-means clustering method and elbow method for identification of the best customer profile cluster. IOP Conf. Ser. Mater. Sci. Eng. 336, 012017.

The UN Refugees Agency, 2022. Emergency Handbook, Camp Site Planning Minimum Standards.

Thorndike, R.L., 1953. Who belongs in the family? Psychometrika 18, 267–276.

Xiao, C.K., Sun, B., Wang, Y.L., Qiu, L.D., 2021. Foreign object detection of sintering transport belt based on CNN. IFAC-PapersOnLine 54, 25–30.

Xie, J., Hu, K., Guo, Y., Zhu, Q., Yu, J., 2021. On loss functions and CNNs for improved bioacoustic signal classification. Ecol. Inf. 64, 101331.

Xu, H., Chen, W., Sun, B., Chen, Y., Chunsheng, L., 2014. Oil tank detection in synthetic aperture radar images based on quasi-circular shadow and highlighting arcs. J. Appl. Remote Sens. 8, 083689.

Yao, Y., Jiang, Z., Zhang, H., 2014. Oil tank detection based on salient region and geometric features. In: Optoelectronic Imaging and Multimedia Technology III, 9273: 92731G. International Society for Optics and Photonics, SPIE.

Zhang, B.Y., Li, H.H., Wang, W., 2015. Numerical study of dynamic response and failure analysis of spherical storage tanks under external blast loading. J. Loss Prev. Process. Ind. 34, 209–217.

Zhang, L., Shi, Z., Jun, W., 2015. A hierarchical oil tank detector with deep surrounding features for high-resolution optical satellite imagery. IEEE J. Sel. Top. Appl. Earth Obs. Rem. Sens. 8, 4895–4909.

Zhang, M., Zheng, F., Chen, F., Pan, W., Mo, S., 2019. Propagation probability of domino effect based on analysis of accident chain in storage tank area. J. Loss Prev. Process. Ind. 62, 103962.

Zhu, R., Hu, X., Bai, Y., Li, X., 2021. Risk analysis of terrorist attacks on LNG storage tanks at ports. Saf. Sci. 137, 105192.